International Journal of Wireless Information Networks (2023) 30:316–331
https://doi.org/10.1007/s10776-023-00606-w

Investigation on the Critical Densification Levels for Coupled and Decoupled User Association in Ultra-dense Networks

Dinkisa Bulti[1] · **Yihenew Wondie**[1]

Received: 30 March 2022 / Revised: 24 April 2023 / Accepted: 14 August 2023 / Published online: 21 September 2023

Abstract

Network densification and heterogeneity has attracted attention as an enabling technology for Fifth Generation (5G) communications due to the potential to enhance capacity using aggressive spatial spectrum reuse and flexibility for deployment. In the framework of Heterogeneous Networks (HetNets), densification is heavy on the pico- or femto-tiers. Therefore, the relative intensity of nodes at each tier impacts the network performance added to the different transmit powers. It could be asked for which densification levels and relative intensity of nodes can we use aggressive offloading with the established interference coordination techniques or decoupled association? In this paper, the concept of Poisson random networks were used to analytically obtain the relative densification levels corresponding to fair load distributions across tiers and intensity levels for which we need the coupled or decoupled User Association UA. The association window, where users choose to use decoupled association in terms of the relative intensity, transmit powers at each tiers and the path loss exponent of the propagation environment, is derived. Further, the ergodic rate expressions in order to study throughput performances in different densification regions, which can be computed numerically, are formulated. To validate the theoretical analysis, numerical, system level simulation and realistic network analysis were used. The analytical, simulation, and realistic test case results provide insights for the operators about the densification ranges, where to use coupled or decoupled association.

Keywords 5G · Heterogeneous networks · Ultra-dense networks · User association · DL and UL decoupling · Cell loads

Abbreviations

1G	First generation
2D	Two dimension
2G	Second generation
3G	Third generation
4G	Forth generation
5G	Fifth generation
3GPP	Third generation partnership project
ABS	Almost blank subframe
ANR	Automatic neighbor relation
ASE	Area spectral efficiency
BBU	Baseband processing unit
BM	Brownian motion
BOA	Bubble oscillation Algorithm
BS	Base station
CA	Carrier aggregation
CAGR	Compound annual growth rate
CAPEX	CAPital EXpenditure
CC	Component carriers
CDF	Commulative distribution function
C-RAN	Cloud-based radio access network
CoMP	Coordinated multi-point
CoV	Coefficient of variation
CP	Critical point
CPs	Critical points
CRE	Cell range expansion
D2D	Device-to-device
DA	Dual association
DL	Downlink
DPM	Dominant path model
DUDe	Downlink and uplink decoupled
eCoMP	Enhanced coordinated multi-point
EE	Energy efficiency
eICIC	Enhanced inter-cell interference coordination
eNodeB	Evolved NodeB
FD	Full duplex
FeICIC	Further enhanced ICIC

✉ Dinkisa Bulti
dinkisa.aga@aait.edu.et

Yihenew Wondie
yihenew.wondie@aait.edu.et

[1] School of Electrical and Computer Engineering, Addis Ababa Institute of Technology, Addis Ababa, Ethiopia

GE	Grammatical evolution
GPS	Geographic positioning system
HD	High definition
HetNets	Heterogeneous networks
HSPA	High speed packet access
ICI	Inter-cell interference
ICIC	Inter-cell intereference coordination
ICT	Information communication technology
IoT	Internet of Things
IP	Internet protocol
ISD	Inter-site distance
KCA	K-means clustering algorithm
LA-OLPS	Load-aware offsetting and adaptive LPS configuration
LPN	Low power node
LPNCR	Low power node center region
LPNER	Low power node edge region
LPS	Low power subframe
LT	Laplace transform
LTE	Long term evolution
LTE-A	Long term evolution advanced
MA	Multiple association
M2M	Machine-to-machine
max-RSS	Maximum received signal strength
MC	Macro cell
MCCR	Macro-cell center region
MCER	Macro-cell edge region
MIMO	Multiple input multiple output
mmWave	Milli-meter wave
MWMP	Maximum weighted matching problem
OFDMA	Orthogonal frequency division multiple access
OPEX	OPerating EXpenditure
P2P	Peer-to-peer
pdf	Probability distribution function
PDL	Power density upper limit
PGFL	Probability generating functional
PF	Proportional fairness
PLE	Path loss exponent
PPP	Poisson point process
QoS	Quality of service
RAN	Radio access network
RAT	Radio access technology
RF	Radio-frequency
RFA	Reverse frequency allocation
RHS	Right-hand side
RR	Round robin
RRH	Remote radio heads
RRM	Radio resource management
RSRP	Reference signal received power
RSRQ	Reference signal received quality
SC	Small cell
SE	Spectral efficiency
SG	Stochastic geometry
SINR	Signal to interference plus noise ratio
SIR	Signal to interference ratio
SNR	Signal to noise ratio
SON	Self-organizing network
TDD	Time division duplexing
UA	User association
UBKCA	User-based K-means clustering algorithm
UDN	Ultra-dense networks
UE	User equipment
UL	Up-link
VNI	Visual networking index
WCDMA	Wideband code division multiple access
Wi-Fi	Wireless fidelty
WIGIG	Wireless gigabit
WiMAX	World wide interoperability for mobile access
WLAN	Wireless local area network

1 Background

In the last four decades, mobile communications have evolved from the First Generation (1G) to the Forth Generation (4G) [1], where traditional communication networks, which mainly focus on voice services, have been gradually revolutionized into multi-functional systems that provide high speed mobile data and other services. In this network evolution, a User Equipment (UE) is associated to the same Base Station (BS) both in Up-Link (UL) and Downlink (DL) [2]. This results in the problem of DL–UL asymmetry in coverage and capacity provisioning in HetNets deployment with different transmit powers between different tiers and UEs. The problem becomes worse in the 5G Ultra-Dense Networks (UDN) [3, 4] deployment because a UE may experience different propagation gains in UL and DL from nearby ultra-dense pico- or femto-BSs. Here, we relate an UDN to an extremely large node density or intensity, which in turn defined as the number of BSs per unit area.

As a promising solution to the aforementioned problem, Downlink and Uplink Decoupled (DUDe) UA scheme has long been area of research. The DUDe UA allows a UE to be associated to Macro Cell (MC) in the DL and to Low Power Node (LPN) in the UL. The flexibility offered with DL and UL decoupling can be used to reduce interference and improve the throughput performance [5, 6].

On the other hand, aggressive offloading [7] of UEs from MC to LPN is the well established approach for load balancing in HetNets with coupled sub-optimal UA. However, as node intensity increases, the serving node becomes much closer to the UE. I.e., the offsetting required would also naturally decrease [8]. Therefore, the relative intensity at each tier can be used to parallel the effect of transmit power differences and to ease the required load balancing effort. The load imbalance in HetNets can also be addressed through flexible DUDe associations [9] that allows to load-balance the DL and UL separately.

Boccardi et al. [2] presented five reasons for why the UL and DL should be decoupled. These reasons are: different load balancing in the UL and DL, low deployment cost, enhanced UL data rate, reduced UL interference and reduced transmit power. In [10], Huang et al. have examined the cell association probability and shown that the load becomes more balanced under DUDe than under coupled association.

Furthermore, Sial and Ahmed [6] have shown that as BS intensities at lower tiers increase, more users prefer DUDe user association. However, in the decoupled scenario, they concluded that there is an upper bound on rise of user performance with respect to node intensity. This is also reported in [11] that as the LPN tier intensity continues to increase, the gains of DUDe do decrease after a certain threshold. The analysis of DUDe for Spectral Efficiency (SE) in a two-tier network by Sattar et al. [12] found that while decoupling can enhance UL performance, the enhancement is still rather insignificant from a system level perspective. The authors came to the conclusion that more thorough analysis is necessary as a result.

Therefore, the effect of relative intensity ratios between HetNets tiers on the rate performance of coupled and decoupled associations needs further investigation. I.e., detailed analysis of ranges of densification levels where we can use coupled association to MC with offloading, decoupled association and coupled association to LPN tier is necessary. In this regard, this paper identifies the densificationn levels at which traffic loads in the UL and DL are independent of the network parameters like transmit power. We call this intensity ratios as *Critical Densification Levels* or Critical Points (CPs), at which we observe fair/equal load distribution among network tiers. Further, we define range of node intensity ratios for which DUDe can be used as decoupling association window.

We use Poisson random networks to analytically obtain the relative densification levels for which we need the coupled assocition with offloading, decoupled and coupled UA. To validate our analysis, numerical and realistic network evaluations are used. We make use of Mathematica and Matlab software tools to compute the closed triple integrals and system level simulations, respectively. Then, using the WinProp software suite, we perform evaluations in a more realistic network environment. Specifically, the work has the following contributions.

- We use a Poisson random network to analytically obtain densification levels at which fair load share exists between tier-1 and tier-2 nodes in the UL and DL for randomly distributed UEs. We refer this densification levels as CPs.
- We derive the association windows, where users choose to use the decoupling association, coupled association with MC or LPN in terms of the relative intensity, transmit powers at each tier and the PLE of the propagation environment.
- We formulate the ergodic rate expressions in order to study throughput performances in different densification regions which can be computed numerically.
- To validate the theoretical analysis, numerical, system level simulation and realistic network analysis are used. Our analytical, simulation, and realistic test case results provide insights for the operators about the densification ranges, where to use coupled or decoupled association.

The rest of the paper is organized as follows. In Sect. 2, we present the related works and detail the research gaps. Then, Sect. 3 presents the system model including the network topology and link model. The fourth section focuses on the derivations of association probabilities and definitions of cell load expressions. We drive critical densification levels which are the concerns of the study. Section 5 presents the formulation of the ergodic rates with proofs presented in Appendix 1. The evaluation settings, analytical and system level simulation results are presented in Sects. 6 and 7 while the last section presents the conclusions.

2 Related Work

An important factor that restricts the UL capacity in dense HetNets is the problem of UL and DL imbalance. As there is a clear disparity between the transmit powers of the MCs and LPNs, the best serving cell for a user may be different in the UL and DL directions. Therefore, if the UL and DL associations are coupled, the UL capacity may be severely limited and this problem will become even worse in the future UDN and milli-meter Wave (mmWave) communications [13].

The work in [14] proposed the DUDe UA framework under a two-tier HetNets, in which the LPNs are randomly located over an MC's coverage area. DUDe framework makes it possible for an UE to select different optimal BSs in DL and UL according to its transmission requirements, which realizes a simultaneous optimal throughput over the two directions. Similarly, Feng et al., in [15] developed a joint UA and resource partition framework for DUDe in a multi-tiered HetNets. Different from the traditional association rules such as Maximum Received Signal Strength (max-RSS) and Cell Range Expansion (CRE), a coalition game based scheme was used for the optimal UA with DUDe. However, these works fail to include all interference contributing factors and overlooks the effect of relative node intensities with respect to different UA schemes.

As the importance of uplink transmission performance has increased with the proliferation of the Internet of Things, it has become more challenging to enhance the system performance of UL in UDN HetNets using the coupled association. In [10], authors compared the UL performance of the DUDe to that of the coupled association in UDN. The numerical result showed that the latency is lower and the energy eeficiency is higher under DUDe than under coupled association. The DUDe performance was also investigated in the case of cellular vehicle-to-everything from the perspective of spectral efficiency (SE) [16]. The result showed better system average SE compared to the coupled association.

The derivation of association probabilities is used to calculate how the capacity is affected when the association is made either with LPN or MC in the UL or DL direction. In [17], the evaluation and comparison of the potential capacity gains of decoupled association of the UL to the LPN with respect to the MC, association that follows classical DL received power rule was performed. Smiljkovikj et al. [5] reported that as the density of the LPNs increases compared to the density of the MCs, a large fraction of UEs chooses to receive from a MC in the DL and transmit to a LPN in the UL. This clearly shows that the effect of further increase in relative node density between different tiers needs investigation.

Sial and Ahmed in [6] and [18], analyzed a UA technique for multi-tier 5G HetNets having dual connectivity and decoupled access or joint DUDe and dual association for spectrum aggregation in UL and DL. They have developed closed form solutions for association, coverage and outage probabilities along with average throughput by considering UL power control, receiver noise and multi-tiers of HetNets. The result shows that with the increase of LPN densities, more UEs prefer decoupled association. However, this preference may reduce in a highly dense HetNets where LPNs density is much more than MCs. They also found that the LPN densities and number of HetNets tiers play a significant role in improving the user performance in joint DUDe and dual association scheme. However, at what LPN density that UE performance starts to decrease was not answered. In [19], it was also reported that identification of the location of the small cell interferer and the LPN offset help in improving the gain that the DUDe can bring to HetNets.

A realistic scenario of a cellular network with different classes of real-world environments was used to analyze performance of a three-tier hybrid mmWave and ultra-high frequency network [20]. The authors investigated gains of DUDe technique. The real-world environment consists of two blockage scenarios: a sub-urban and a denser setting. However, the propagation model used may not give accurate result compared to the ray-tracing method.

To differentiate between deployment scenarios for which we can use coupled or decoupled association, investigation of the relation between performance and cell density is important. The authors in [11] studied the dependency of DUDe performance with LPN density in two-tier network with 2×2 Multiple Input Multiple Output (MIMO) at each tier. The result shows that increasing the number of LPNs largely improves the performance of UEs initially but the gains are marginal after a certain density of LPNs. The question "What is this critical density level that marginal effect on throughput occurs?" must be investigated.

3 System Model

3.1 Network Topology

We consider a two-tier network where BSs at each tier are located according to the homogeneous Poisson Point Process (PPP) represented by Φ_m and Φ_l with intensities (equivalently, densities) of λ_m and λ_l respectively for MC-tier and LPN-tier. A typical spatial coverage layout of the two-tier network deployment under consideration is shown using a Voronoi tessellation with a normalized scale in Fig. 1.

We let the set of MCs denoted by $\mathcal{N}_m = \{BS_j : j = 1, 2, 3, \ldots, N_m\}$, set of LPNs denoted by $\mathcal{N}_l = \{lpn_j : j = 1, 2, 3, \ldots, N_l\}$ and a typical UE located at the center of the region $\mathcal{A}$ under consideration denoted by u. We also assume UEs are located in the region according to the PPP denoted by Φ_u with intensity λ_u. The list and descriptions of the notations and parameters are provided in Table 1.

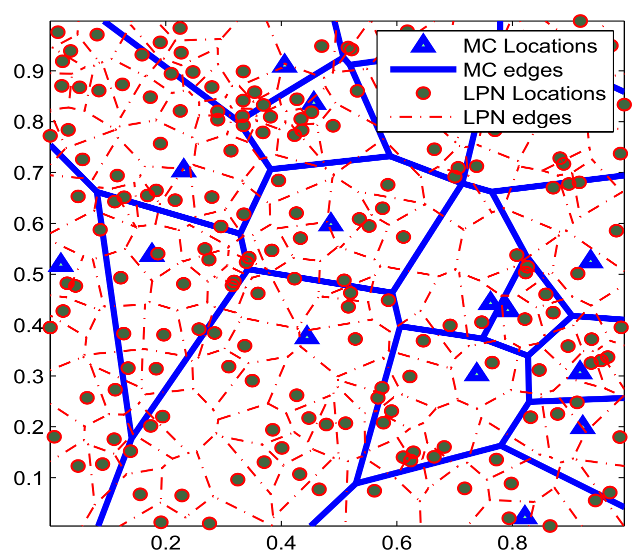

Fig. 1 A view of Two-tier Poisson Random Network Deployment with cell boundaries corresponding to a Voronoi Tessellation with Normalized Dimensions

Table 1 Notations and list of parameters

Notations	Descriptions
N_m, N_l, and U	Number of MCs, LPNs, and UEs, respectively
$\mathcal{N}_m$, and $\mathcal{N}_l$	Set of MCs, and LPNs, respectively
Φ_m, Φ_l, and Φ_u	The PPP of MC, LPN, and UE locations, respectively
λ_m, λ_l, λ_u	Intensity of MCs, LPNs, and UEs, respectively
A	Two-dimensional area under considerations
u	A UE at the center
P_k	Transmit power for $k \in (u, \mathcal{N}_m, \mathcal{N}_l)$
P_k^{rx}	Received power at UE or BS locations
α	Intensity ratio between λ_l and λ_m
r_k	Distance of BS from the center
γ_k	Path loss exponent for $k \in (u, \mathcal{N}_m, \mathcal{N}_l)$
h_k	Exponential channel gain with mean $1/\mu$
$\overline{\gamma}$	Ratio of PLE
$\overline{P}$	Transmit power ratio
ψ	Instantaneous SINR
$\mathbf{P}$	Probability
$\mathbf{E}$	Expectation of a random variable
δ	Cell load
S^k	Resource of the kth cell
s^k	Allocated resource units
n^k	Number of associated UEs to the kth BS
R_z	Ergodic rate for $z \in (DL, UL, DL/UL)$
v	Association variable
$\mathcal{L}$	Laplace Transform

3.2 Link Model

For the link model, we assume that there is no intra-cell interference between users within the same cell as they can be assigned non-interfering set of resource blocks. However, users could suffer from inter-cell interference. We denote the transmit power by P_k where k can be either the UE, MCs or LPNs, i.e., $k \in \{u, \mathcal{N}_m, \mathcal{N}_l\}$. In this case, the received power, P_k^{rx} at u or BS location in DL/UL at distance r_k from the serving BS is $P_k h_k r_k^{-\gamma_k}$, where h_k is a random variable that follows an exponential distribution with mean $1/\mu$, i.e., $h_k \sim \exp(\mu)$ and γ_k is path loss exponent.

The probability distribution function (pdf) of the distance $f(r, n)dr$ from an arbitrarily chosen origin (where a typical user u is supposed to be placed) to the nth nearest neighbor in the case of PPP is expressed as in (1) [21]:

$$f(r,n)dr = \frac{2(\pi\lambda_k)^n}{(n-1)!} r^{2n-1} e^{-\pi\lambda_k r^2} dr; \quad r > 0; n = 1, 2, 3, \ldots \tag{1}$$

Using the same expressions in [14], but considering a large number of MC and the interfering UE transmissions in the UL; both distributed according to the independent PPP, the Signal to Interference Plus Noise Ratio (SINR), ψ expressions from the UE at the center to the serving MC or LPN in the DL and UL at a distance r is given as in (2a)–(2d). Here, since the network will be interference limited the noise power can be neglected.

$$\psi_{UL}^m(r) = \frac{P_u h_m r^{-\gamma_m}}{\sum_{k\in\Phi_u\backslash u} P_u h_k r^{-\gamma_k}} \tag{2a}$$

$$\psi_{UL}^l(r) = \frac{P_u h_l r^{-\gamma_l}}{\sum_{k\in\Phi_u\backslash u} P_u h_k r^{-\gamma_k}} \tag{2b}$$

$$\psi_{DL}^m(r) = \frac{P_m h_m r^{-\gamma_m}}{\sum_{k\in\Phi_m\backslash m} P_m h_k r^{-\gamma_k} + \sum_{k\in\Phi_l} P_l h_k r^{-\gamma_k}} \tag{2c}$$

$$\psi_{DL}^l(r) = \frac{P_l h_l r^{-\gamma_l}}{\sum_{k\in\Phi_m} P_m h_k r^{-\gamma_k} + \sum_{k\in\Phi_l\backslash l} P_l h_k r^{-\gamma_k}} \tag{2d}$$

4 User Association and Critical Levels of Densification

In this section, we derive expressions for the UL and DL association probabilities and joint association probabilities. We make use of similar analytical derivation approaches using Poisson random network as in [5, 6, 15] and other literature for illustration and completeness of our discussion and provide tractable procedure for the readers. Our steps clearly show the approach to identify critical densification levels and intensity ranges for decoupled and coupled user associations, which makes it different from aforementioned references. Also, we present the definitions and expressions for cell loads to be used later in the numerical evaluation.

4.1 DL and UL Association Probabilities

We begin with the UL association probabilities. The UL association probability of a user to an MC can be obtained considering the long term average received power based association as in (3).

$$
\begin{aligned}
\mathbf{P}_{UL}^{m} =& \mathbf{E}_{r_m}[\mathbf{P}\{\mathbf{E}_h[P_u h_l r_l^{-\gamma_l}] < \mathbf{E}_h[P_u h_m r_m^{-\gamma_m}]\}] \\
\overset{a}{=}& \mathbf{E}_{r_m}[\mathbf{P}\{r_l^{-\gamma_l} < r_m^{-\gamma_m}\}] \\
=& \mathbf{E}_{r_m}[\mathbf{P}\{r_l > r_m^{\overline{\gamma}}\}] \\
\overset{b}{=}& \mathbf{E}_{r_m}[\exp\{-\pi\lambda_l r^{2\overline{\gamma}}\}] \\
=& \int_0^\infty \exp\{-\pi\lambda_l r^{2\overline{\gamma}}\} f_{r_m}(r,1) dr \\
=& \int_0^\infty 2\pi\lambda_m r \exp\{-\pi\lambda_l r^{2\overline{\gamma}}\}\exp\{-\pi\lambda_m r^2\} dr,
\end{aligned} \tag{3}
$$

where $\overline{\gamma} = \frac{\gamma_m}{\gamma_l}$. Here, the best serving MC is at distance r_m from the user and the nearest LPN is located at a distance of r_l. The $f_{r_m}(r,1)$ is the pdf of the distance between a UE and the serving MC. (a) follows from the exponential distributed h_k with mean $1/\mu$ and the same UL transmit power of a user and (b) follows from the probability that no particle is found in a disk of area πr^2 in a two-dimensional PPP with intensity λ is $\exp\{-\pi\lambda r^2\}$.

For $\overline{\gamma} = 1$, the probability that a UE at the origin is associated to the MC-tier is

$$
\mathbf{P}_{UL}^{m} = \frac{\lambda_m}{\lambda_m + \lambda_l} = \frac{1}{1+\alpha}, \tag{4}
$$

where $\alpha = \frac{\lambda_l}{\lambda_m}$ and the proof is as follows. Substituting the integration variable with $x = -\pi\lambda_m r^2$ and $dx = -2\pi\lambda_m r dr$ then, integrating and re-substitution in (5) gives the result in (4).

$$
\begin{aligned}
\mathbf{P}_{UL}^{m} &= -\int \exp\left\{x\frac{\lambda_m+\lambda_l}{\lambda_m}\right\}dx \\
&= \frac{-\lambda_m}{\lambda_m+\lambda_l}\exp\left\{-\pi(\lambda_m+\lambda_l)r^2\right\}\Big|_0^\infty
\end{aligned} \tag{5}
$$

From (4), the UL association probability of a user to a LPN can be obtained as:

$$
\begin{aligned}
\mathbf{P}_{UL}^{l} &= 1 - \mathbf{P}_{UL}^{m} \\
&= \frac{\alpha}{1+\alpha}
\end{aligned} \tag{6}
$$

In a similar process, the DL probability that a UE is associated to the MC or LPN can be expressed as:

$$
\begin{aligned}
\mathbf{P}_{DL}^{m} =& \int_0^\infty 2\pi\lambda_m r \\
& \exp\left\{-\pi\lambda_l(\overline{P}^{\frac{-2}{\gamma_l}} r^{2\overline{\gamma}})\right\}\exp\{-\pi\lambda_m r^2\}dr \\
& \text{and} \\
\mathbf{P}_{DL}^{l} =& \int_0^\infty 2\pi\lambda_m r(1-\exp\{-\pi\lambda_l(\overline{P}^{\frac{-2}{\gamma_l}} r^{2\overline{\gamma}})\} \\
& \exp\{-\pi\lambda_m r^2\})dr,
\end{aligned} \tag{7}
$$

where $\overline{P} = \frac{P_m}{P_l}$ and integrating over the interval for $\overline{\gamma} = 1$ gives:

$$
\begin{aligned}
\mathbf{P}_{DL}^{m} =& \frac{1}{\alpha\overline{P}^{\frac{-2}{\gamma_l}}+1} \\
& \text{and} \\
\mathbf{P}_{DL}^{l} =& \frac{\alpha\overline{P}^{\frac{-2}{\gamma_l}}}{\alpha\overline{P}^{\frac{-2}{\gamma_l}}+1}
\end{aligned} \tag{8}
$$

Using (4), (6) and (8), we can state Lemma 1 as follows for equal load distribution between MC- and LPN-tiers.

Lemma 1 (Points of fair load distribution) *For a given PLE $\gamma_l = \gamma_m$ and transmit power ratio $\overline{P}$, the DL equal load share is obtained at $\alpha^* = \overline{P}^{\frac{2}{\gamma_l}}$ while that of the UL is obtained at $\alpha^* = 1$.*

Proof From (4) and (6), the UL equal association probability to the MC and LPN is obtained when $\mathbf{P}_{UL}^{m} = \mathbf{P}_{UL}^{l} = 0.5$ which is for $\alpha^* = 1$. For the DL equal association probability to the MC and LPN, we equate $\mathbf{P}_{DL}^{m}$ and $\mathbf{P}_{DL}^{l}$ of (8) and solving for α gives $\alpha^* = \overline{P}^{\frac{2}{\gamma_l}}$.

The relative node intensity range between $\alpha^* = 1$ and $\alpha^* = \overline{P}^{\frac{2}{\gamma_l}}$ represents the region of DL and UL load imbalance. Further, it can be observed that as tier-2 intensity increases or for $\alpha >> \alpha^*$, the UE tends to attach itself to the LPN-tier. Also note that the UL association probability is only affected by the relative density of nodes at both tiers not by the transmit power. In addition to the relative density of nodes, the DL association probability is also affected by both the transmit power at each tier and the PLE. Consider two PLEs $\gamma_l = 2$ and $\gamma_l = 4$ corresponding to rural and dense urban propagation environments, respectively. For a given transmit power ratio $\overline{P} = \frac{P_m}{P_l}$ (assuming $P_m > P_l$), the critical point of equal probability of association (α^*) is smaller when γ is larger. I.e., the load imbalance due to the large transmit power of the MC-tier can get better of at a smaller node intensity ratio α as shown in Fig. 2. In the figure, we label CP1, CP2 or CP3 to indicate critical points of equal association probability in the DL for $\gamma = 4$, 3, or 2, respectively.

4.2 Joint User Association Probabilities

The joint probability of UA in the UL and DL to the MC-tier or LPN-tier offers the opportunity to define the coupled and decoupled association regions. We identify three scenarios as in [5]:

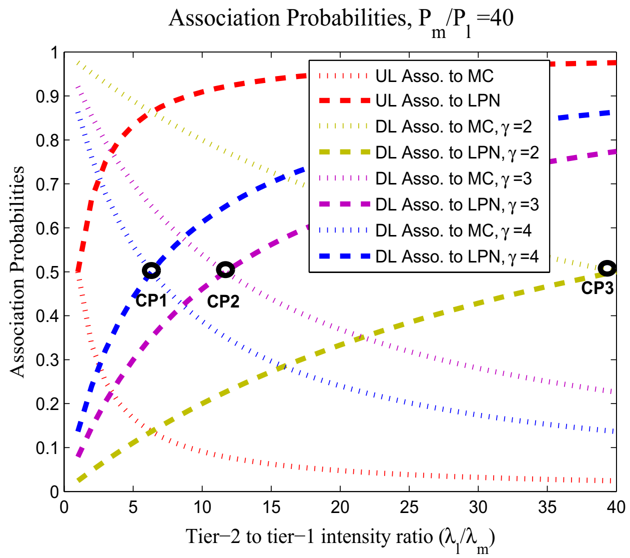

Fig. 2 User association probabilities in the UL and DL for different path loss exponents

- Case 1: User associated to MC both in the DL and UL or coupled association with MC (called Coupled-MC afterwards).
- Case 2: User associated to LPN both in the DL and UL or coupled association with LPN (called Coupled-LPN afterwards).
- Case 3: User associated to MC in the DL and to the LPN in the UL or decoupled association.

The association to the LPN in the DL and to the MC in the UL will not happen since user always tends to attach itself to the LPN in the UL as far as $\lambda_l \gg \lambda_m$ and to the MC in the DL for $P_m \gg P_l$. Here, Case 1 & 2 define the coupled association while Case 3 is for UL and DL decoupled association.

Case 1: Coupled Association (Coupled-MC)

The probability that a user will be associated to the MC-tier in both DL and UL is obtained from:

$$\begin{aligned}
&\mathbf{P}^{m}_{DL/UL} \\
&= \mathbf{E}_{r_m}[\mathbf{P}\{\mathbf{E}_{h_l}[P_u h_l r_l^{-\gamma_l}] \leq \mathbf{E}_{h_m}[P_u h_m r_m^{-\gamma_m}] \\
&\bigcap \mathbf{E}_{h_m}[P_m h_m r_m^{-\gamma_m}] \geq \mathbf{E}_{h_l}[P_l h_l r_l^{-\gamma_l}]\}] \\
&\overset{a}{=} \mathbf{E}_{r_m}[\mathbf{P}\{r_l^{-\gamma_l} \leq r_m^{-\gamma_m} \bigcap P_m r_m^{-\gamma_m} \geq P_l r_l^{-\gamma_l}\}] \\
&= \mathbf{E}_{r_m}[\mathbf{P}\{r_l^{-\gamma_l} \leq r_m^{-\gamma_m}\}] \\
&= \frac{1}{1+\alpha}.
\end{aligned} \tag{9}$$

In (9), (a) follows from the exponentially distributed gain h and taking the intersection completed the derivation.

Case 2: Coupled Association (Coupled-LPN)

Similarly, for the Case 2, the probability that a user will be associated to the LPN-tier in both DL and UL is obtained from the condition in (10) and is given in (11):

$$\begin{aligned}
\mathbf{P}^{l}_{DL/UL} =& \mathbf{E}_{r_l}[\mathbf{P}\{\mathbf{E}_{h_l}[P_u h_l r_l^{-\gamma_l}] \geq \mathbf{E}_{h_m}[P_u h_m r_m^{-\gamma_m}] \\
&\bigcap \mathbf{E}_{h_m}[P_m h_m r_m^{-\gamma_m}] \leq \mathbf{E}_{h_l}[P_l h_l r_l^{-\gamma_l}]\}]
\end{aligned} \tag{10}$$

$$\mathbf{P}^{l}_{DL/UL} = \frac{\alpha \bar{P}^{\frac{-2}{\gamma_l}}}{\alpha \bar{P}^{\frac{-2}{\gamma_l}} + 1} \tag{11}$$

From (9), and (11), it can be observed that the coupled association to the MC-tier is dominated by the UL long-term averaged received power while the coupled association to the LPN-tier is dictated by the DL long-term averaged received power.

Case 3: Decoupled Association

For the decoupled association, we consider UL association to the LPN-tier and DL association to the MC-tier. The association probability is obtained from the condition in (12) and is given in (13).

$$\begin{aligned}
\mathbf{P}^{m/l}_{DL/UL} =& \mathbf{E}_{r_m}[\mathbf{P}\{\mathbf{E}_{h_l}[P_u h_l r_l^{-\gamma_l}] \geq \mathbf{E}_{h_m}[P_u h_m r_m^{-\gamma_m}] \\
&\bigcap \mathbf{E}_{h_m}[P_m h_m r_m^{-\gamma_m}] \geq \mathbf{E}_{h_l}[P_l h_l r_l^{-\gamma_l}]\}]
\end{aligned} \tag{12}$$

$$\mathbf{P}^{m/l}_{DL/UL} = \frac{\alpha}{1+\alpha} - \frac{\alpha \bar{P}^{\frac{-2}{\gamma_l}}}{\alpha \bar{P}^{\frac{-2}{\gamma_l}} + 1} \tag{13}$$

Lemma 2 (Decoupling association window) *The maximum probability for decoupled association is found at* $\alpha = \bar{P}^{\frac{1}{\gamma_l}}$ *and the maximum decoupling association window is between* $\frac{\bar{P}^{\frac{2}{\gamma_l}}}{\bar{P}^{\frac{2}{\gamma_l}}-2} \leq \alpha \leq \bar{P}^{\frac{2}{\gamma_l}} - 2.$

Proof The maximum probability for decoupled association can be readily obtained by taking the first derivative of (13). Then, equating to zero and solving for α gives the result. Since (13) is a concave function of α, the decoupling association window can be proved by evaluating the inequality $\mathbf{P}^{m/l}_{DL/UL} \geq \mathbf{P}^{m}_{DL/UL}$ and $\mathbf{P}^{m/l}_{DL/UL} \geq \mathbf{P}^{l}_{DL/UL}$. Substituting from (9), (11), and (13), and solving for α readily gives $\frac{\bar{P}^{\frac{2}{\gamma_l}}}{\bar{P}^{\frac{2}{\gamma_l}}-2} \leq \alpha \leq \bar{P}^{\frac{2}{\gamma_l}} - 2.$

Observe that the decoupling association window is lower and upper bounded by points of UL and DL fair load distributions of Lemma 1, respectively. I.e., $\alpha^* = 1 < \frac{\bar{P}^{\frac{2}{\gamma_l}}}{\bar{P}^{\frac{2}{\gamma_l}}-2}$ and $\bar{P}^{\frac{2}{\gamma_l}} - 2 < \bar{P}^{\frac{2}{\gamma_l}} = \alpha^*$. Furthermore, for $\gamma_l = \gamma_m = 4$ and

$\overline{P} = 40$, the maximum probability for decoupled association is found approximately at $\alpha = 2.5$.

Therefore, from preceding Lemmas 1 and 2, we can state the main result as in Theorem 1 without proof as it is a direct consequence of the previous discussions.

Theorem 1 (Coupled and Decoupled Association Regions): *Based on the critical densification levels and decoupling association window given above, we have the following three regions for flexible user association.*

1. $0 < \alpha < \frac{\overline{P}^{\frac{2}{\gamma_l}}}{\overline{P}^{\frac{2}{\gamma_l}}-2}$ - *Coupled association to MC; possibly with offloading*
2. $\frac{\overline{P}^{\frac{2}{\gamma_l}}}{\overline{P}^{\frac{2}{\gamma_l}}-2} \leq \alpha \leq \overline{P}^{\frac{2}{\gamma_l}} - 2$ - *Decoupled association*
3. $\alpha > \overline{P}^{\frac{2}{\gamma_l}} - 2$ - *Coupled association to the LPN*

4.3 Number of Users Per Cell and Cell Loads

The number of users associated to the MC-tier in the DL is $|U|^m_{DL} = \mathbf{P}^m_{UL} \cdot |U|$, where $|U|$ is the total number of users. If we denote N_m as number of nodes in the MC-tier on area of $\mathcal{A}$, the number of users per cell can be obtained as:

$$\begin{aligned} n^m_{DL} =& \frac{|U|^m_{DL}}{N_m} = \frac{\mathbf{P}^m_{DL} \cdot |U|}{\lambda_m \mathcal{A}} \\ =& \frac{\mathbf{P}^m_{DL} \cdot \lambda_u}{\lambda_m} \end{aligned} \tag{14}$$

The number of users associated to a cell in MC-tier in the UL is given as:

$$\begin{aligned} n^m_{UL} =& \frac{|U|^m_{UL}}{N_m} = \frac{\mathbf{P}^m_{UL} \cdot |U|}{\lambda_m \mathcal{A}} \\ =& \frac{\mathbf{P}^m_{UL} \cdot \lambda_u}{\lambda_m} \end{aligned} \tag{15}$$

Similarly, the number of users per cell associated to LPN in the DL and UL are respectively given by:

$$\begin{aligned} n^l_{DL} =& \frac{\mathbf{P}^l_{DL} \cdot \lambda_u}{\lambda_l} \\ & \text{and} \\ n^l_{UL} =& \frac{\mathbf{P}^l_{UL} \cdot \lambda_u}{\lambda_l}. \end{aligned} \tag{16}$$

The cell load at each tier can be estimated assuming a general resource definition as follows. Let us denote a resource of a cell as S^k, where $k \in \{m, l\}$ from which s^k-units can be allocated to a user using Round Robin scheduling. Therefore, the average cell load at the jth BS of kth-tier is given by

$$\delta^k_j = \frac{s^k \cdot n^k_{DL/UL}}{S^k}. \tag{17}$$

5 DL and UL Ergodic Rates

The achievable rate in the UL and DL for UEs associated with the MC or LPN can be obtained as a product of the association probabilities for the three cases and the achievable rate according to the Shannon's formula. Let v denote association to MC or LPN, i.e., $v \in \{m, l, m/l\}$ and z denote the direction, i.e., $z \in \{DL, UL, DL/UL\}$. Then, the ergodic rate R_z is obtained as follows:

$$R_z = R^v_z \cdot \mathbf{P}^v_z = \frac{1}{\ln(2)} \mathbf{E}_{r,\psi}[\ln(1 + \psi(r)^v_z)] \cdot \mathbf{P}^v_z \tag{18}$$

Here, we state the ergodic rates when a typical UE is associated to the MC or LPN in the UL or DL. To obtain the ergodic rates, we assume the interference in the UL is from all UEs transmitting to the LPNs or MCs except the UE at the origin; all of them scheduled on the same resource blocks. In the worst case, the number of interfering UEs scheduled on the same resource blocks becomes $N_m + N_l - 1$. We model this number of interfering UE as thinning of the original PPP with intensity λ^*_u and Lemma 3 gives the ergodic rates when the user is associated to the MC or LPN in the UL and the proof is provided in Appendix 1.

Lemma 3 (The UL ergodic rates)

$$\begin{aligned} R^m_{UL} =& \frac{1}{\ln(2)} \int_0^\infty \int_0^\infty 2\pi\lambda_m r \exp\{-2\pi\lambda^*_u \int_r^\infty (1- \\ & \frac{1}{r^{\gamma_m}(e^y - 1)x^{-\gamma_k} + 1})\} \\ & \exp(-\pi\lambda_m r^2) x dx dr dy \\ & R^l_{UL} = \frac{1}{\ln(2)} \int_0^\infty \int_0^\infty 2\pi\lambda_l r \exp\{-2\pi\lambda^*_u \int_r^\infty (1- \\ & \frac{1}{r^{\gamma_l}(e^y - 1)x^{-\gamma_k} + 1})\} \\ & \exp(-\pi\lambda_l r^2) x dx dr dy \end{aligned} \tag{19}$$

For the DL ergodic rate, we assume the interference is caused by all nodes of both tiers except the serving node. The expression is stated in Lemma 4 and the proof is provided in Appendix 2.

Lemma 4 (The DL ergodic rates)

$$
\begin{aligned}
R^m_{DL} =& \frac{1}{\ln(2)} \int_0^\infty \int_0^\infty \{\exp\{-2\pi\lambda_m \int_r^\infty (1- \\
& \frac{1}{r^{\gamma_m}(e^y-1)x^{-\gamma_k}+1})xdx\} \\
& \times \exp\{-2\pi\lambda_l \int_r^\infty (1-\frac{1}{\overline{P}^{-1} r^{\gamma_m}(e^y-1)z^{-\gamma_k}+1}) \\
& zdz\}\}f(r,1)drdy \\
R^l_{DL} =& \frac{1}{\ln(2)} \int_0^\infty \int_0^\infty \{\exp\{-2\pi\lambda_l \int_r^\infty (1- \\
& \frac{1}{r^{\gamma_l}(e^y-1)x^{-\gamma_k}+1})xdx\} \\
& \times \exp\{-2\pi\lambda_m \int_r^\infty (1-\frac{1}{\overline{P}r^{\gamma_l}(e^y-1)z^{-\gamma_k}+1}) \\
& zdz\}\}f(r,1)drdy
\end{aligned}
\tag{20}
$$

From the discussion in Sect. 3 and (18), the UL and DL throughput performances depend on the association probabilities of UE to the LPN and MC and link rates.

6 System Level Simulation and Numerical Evaluations

6.1 Cell Loads

In this section, we perform numerical evaluations and system level simulation on the densification level with respect to cell load distribution among BSs of the network.

The cell loads with respect to the intensity ratio between λ_l and λ_m for DL and UL associations to the MC and LPN, where $\gamma = 4$ were considered. From Fig. 2, a DL equal load distribution is obtained at the Critical Point (CP) of $\alpha^* = \overline{P}^{\frac{2}{\gamma_l}}$. It was observed that an UL equal load share point appears before α^* because of the asymmetry between DL and UL. It was also shown that the DL CP shifts to the right as we decrease the PLE. With larger PLE, the case in dense urban deployment scenario, more UEs tend to associate with LPNs and the CP shift to the left.

In Figs. 3, 4 and 5, we present the average cell load distribution with respect to the ratio of user to tier-1 and tier-2 intensity considering three densification levels: before, at the CP and after CP. Here, both tier-1 and tier-2 intensities are kept constant and the user intensity is varied.

At densification levels before the CP, cell loads on the MC-tier is higher in the DL. This densification level is where the DL transmit power of the MC-tier dominates and UEs tend to associate with tier-1. Therefore, it is where we need load-aware and cell-specific offsetting and adaptive inter-cell interference coordination.

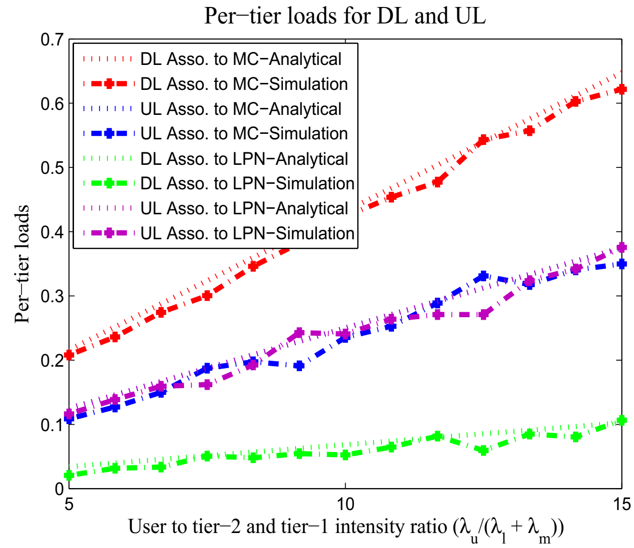

Fig. 3 Per-tier Loads with respect to the ratio of User to tier-2 or tier-1 intensity, at UL-DL equal prob. (before CP1)

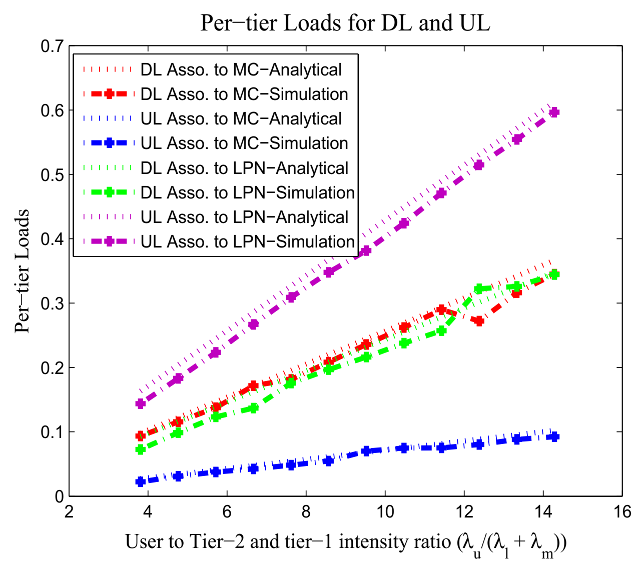

Fig. 4 Per-tier Loads with respect to the ratio of User to tier-2 or tier-1 intensity, at the CP1

In the case of densification level at the CP1 of Fig. 2, we observe from Fig. 4 that although UE intensity λ_u grows with regard to the nodes intensity λ_l and λ_m, the DL load on MC-tier and LPN-tier increase at the same rate and remains fairly equal.

After CP, the reverse happens, where the DL cell loads on the LPN-tier becomes significant. Here, the number of UEs, which prefer to associate with LPNs, is much higher compared to the number of UEs which prefer to associate with MCs, both in the DL and UL. Hence, users tend to

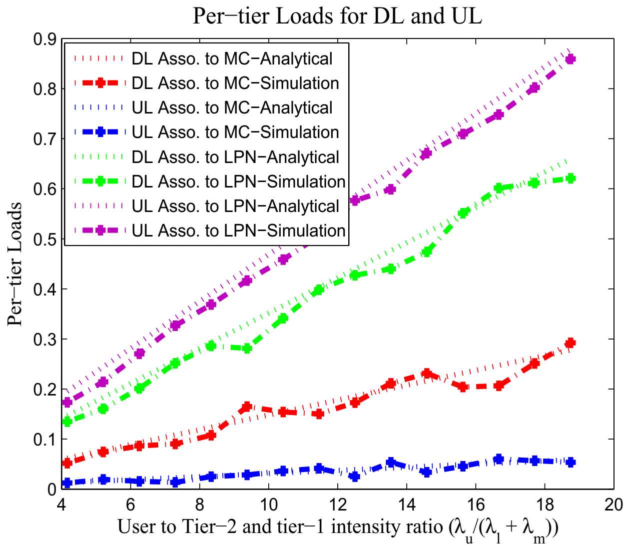

Fig. 5 Per-tier Loads with respect to the ratio of User to tier-2 or tier-1 intensity, after CP1

associate with LPN when $\alpha \gg \alpha^*$ and tier-2 BSs become loaded.

6.2 Average User rate

The triple integrals in (19) and (20) were integrated using the software tool Mathematica. Then, (18) was evaluated and the result was linked with Matlab, using Mathematica's 'matlink' application for further inquiry.

The UL link rate for the three cases with respect to the tier-2 intensity is shown in Fig. 6. The result is plotted for $\gamma_l = 4$, $\lambda_m = 4/Km^2$, link rate threshold $y = 5bps/Hz$ and a channel bandwidth $s^k = 180KHz$.

As can be seen, for smaller relative intensity $\alpha < \frac{\overline{P}^{\frac{2}{\gamma_l}}}{\overline{P}^{\frac{2}{\gamma_l}}-2}$ coupled association to the MC gives better user throughput. As tier-2 intensity starts to increase, i.e., $\frac{\overline{P}^{\frac{2}{\gamma_l}}}{\overline{P}^{\frac{2}{\gamma_l}}-2} \leq \alpha \leq \overline{P}^{\frac{2}{\gamma_l}} - 2$, UEs with decoupled association (case 3) gets better throughput. However, for $\alpha > \overline{P}^{\frac{2}{\gamma_l}} - 2$ coupled association to the tier-2 gives higher user throughput compared the other scheme. Also, notice that the decoupled association window gets decreased with increase of the PLE.

Figure 7 shows the DL link rate for the three cases with respect to the tier-2 intensity. The result is again plotted for $\gamma_l = 4$, $\lambda_m = 4/Km^2$, link rate threshold $y = 5bps/Hz$ and a channel bandwidth $s^k = 180KHz$. Similar to the UL, coupled association to the MC gives better DL user throughput for smaller relative intensity $\alpha < \frac{\overline{P}^{\frac{2}{\gamma_l}}}{\overline{P}^{\frac{2}{\gamma_l}}-2}$ compared to case 2 and case 3. As tier-2 intensity starts to increase, i.e., $\frac{\overline{P}^{\frac{2}{\gamma_l}}}{\overline{P}^{\frac{2}{\gamma_l}}-2} \leq \alpha \leq \overline{P}^{\frac{2}{\gamma_l}} - 2$, UEs with decoupled association (case 3) receive better throughput. But, for $\alpha > \overline{P}^{\frac{2}{\gamma_l}} - 2$ coupled association to the tier-2 gives higher user throughput. The numerical results for both the DL and UL support Theorem 1 as the highest throughput performances correspond to the most likely association cases in different densification regions.

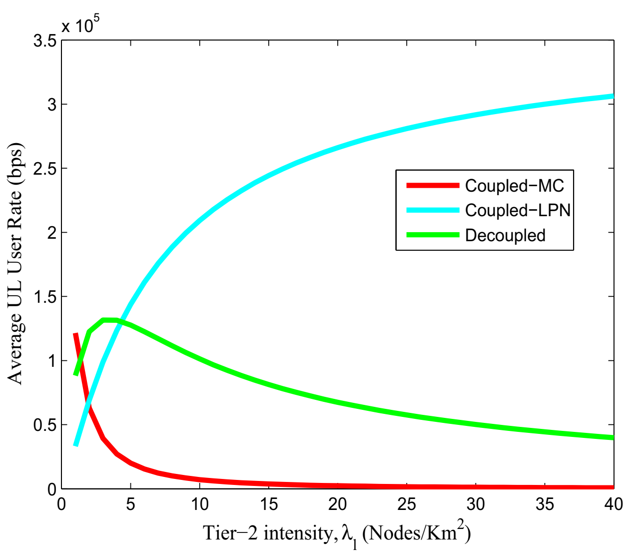

Fig. 6 The UL User Rate for: Case 1(RED), Case 2(CYAN) and Case 3 (GREEN) (Color figure online)

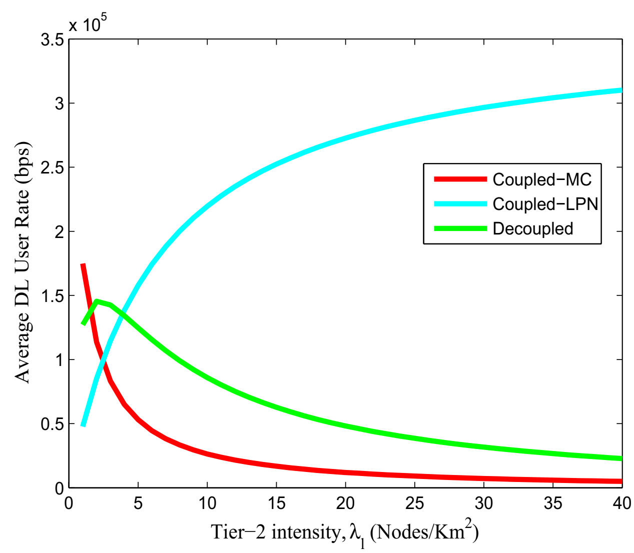

Fig. 7 The DL User Rate for: Case 1(RED), Case 2(CYAN) and Case 3(GREEN) (Color figure online)

7 Test Cases in Realistic Scenario

In this section, we will go through the details on how the system level simulator parameters are configured and used. The use of a digital map is discussed. The deployment scenario is described in detail. The application of a ray-tracing-based signal map generating tool is also discussed. After that, the simulation results are presented and discussed.

7.1 Simulator Settings

A realistic scenario in Addis Ababa is considered (particularly, the Arat-kilo and Amist-kilo areas). This permits a comparison to be made between the numerical evaluation findings and the output that an operator could receive during deployment.

This scenario is used for comparison purpose with the previous numerical results in Figs. 6 and 7. Hence, this scenario was designed to be analogous to the realistic one in its dimensions and number of MCs or LPNs. There are four MCs and a configurable number of LPNs in the realistic scenario. The locations of the MCs are taken from the existing deployment. As a densification layer, the LPNs are used. They are stationed on street corners and in strategic locations as hotspot service areas.

Map and Transmitter Descriptions

The digital map for Arat-kilo and Amist-kilo area is used covering an area of around 1000m by 1000m. The deployment area with the topography and building map shown in Fig. 8a. The terrain elevation of the area varies from 2430m - 2490m and the building heights vary from 4m-45m. We do not consider trees as its effect is assumed to be insignificant. A typical deployment scenario is shown in Fig. 8b.

Path loss and simulator

As the realistic scenario represent the existing deployment, for the path loss and signal map computation, we consider both sectored and omni-directional transmitters. The received power and path losses are predicted at a receiver height of 1.5m from the ground for all transmitters. From the radio propagation and network planning tool WinProp, we used the Dominant Path Model (DPM) to generate the signal map, which guarantees accurate and confident results. Other important information on the transmitter settings are given in Table 2.

The Matlab based system level simulator generates signal map using selected path loss model. It also generates user location map and compute the received signal strength at each UE locations. The path loss at each pixel in the considered computation area generated from DPM is further processed using Matlab based simulator which is also used to implement other empirical path loss models.

7.2 Results and Analysis

We consider two performance metrics: cell-average and cell-edge user data rates. For both metrics, we consider different densification intensities such that a comparison can be drawn with the numerical results presented in the previous section.

Cell-average user data rates

Since the test for exhaustive range of intensity level is difficult in the realistic scenario, strategic study was employed and four densification levels are considered (see Figs. 9 and 10). These are intensity before the critical point, CP1 (or $\alpha = 1$), intensity at maximum probability of DUDe association (or approximately $\alpha = 2.5$), around the edge of the decoupled association window (or $\alpha = 4$) and beyond CP1

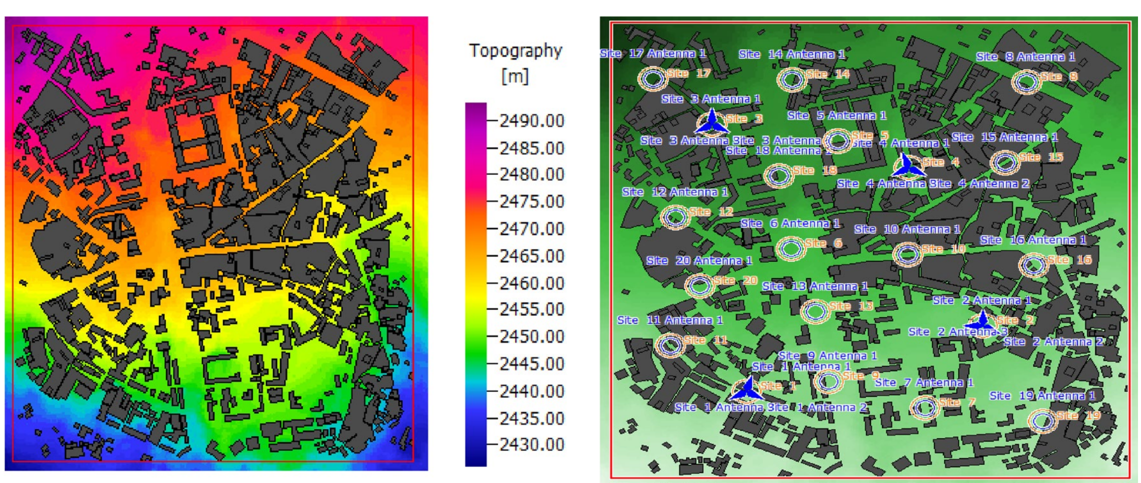

(a) Topography and building map (b) Deployment Scenario of Test case area

Fig. 8 Deployment area **a** topography and building map **b** Deployment scenario

Table 2 Simulation parameters and values

Parameters/descriptions	Values
Downlink transmit power	MC: 46 dBm, LPN: 30 dBm
Uplink transmit power	20 dBm
Center frequency	1800 Mhz
Bandwidth	20 Mhz
Simulation area	1000 x 1000 m^2
Number of snapshots	300
Spatial UE distribution models	Uniform distribution
Antenna heights	MC: 30m, LPN: 5m, UE:1.5m
Tx antenna	MC: Sectored, gain = 0dBi,
	LPN: Omni-directional, gain= 0dBi
Rx antenna gain	0dBi
Path loss model	DPM for realistic deployment
	$PL = A + 10\gamma \log(d/d_0)$, Fixed reference model [22]
	$d_0 = 1m, \gamma = 3-4$ for Matlab-based simulator only
Noise power	−173 dBm/hz
Deployment scenario	4 Macro-sites, variable number of LPNs

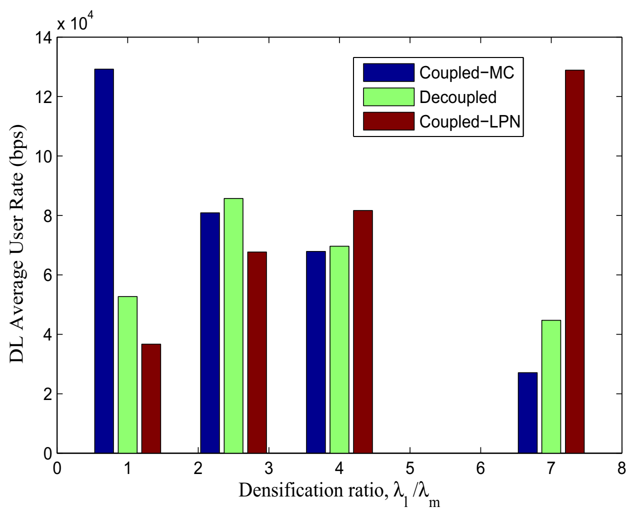

Fig. 9 DL cell-average user rate at different densification ratios, $\lambda_m = 4/Km^2$

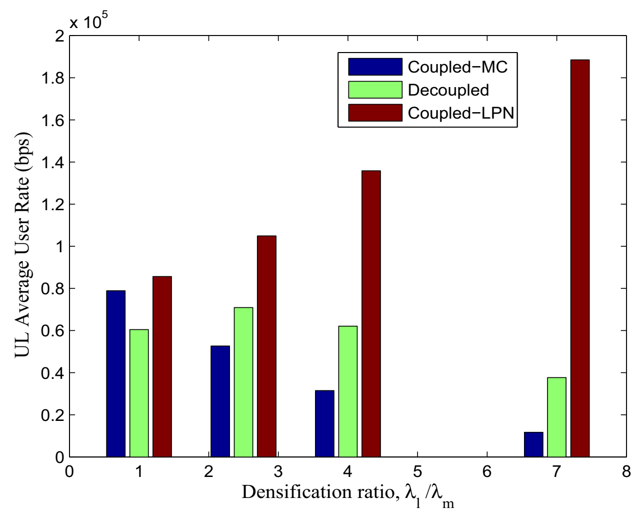

Fig. 10 UL cell-average user rate at different densification ratios, $\lambda_m = 4/Km^2$

(or $\alpha = 7$). These intensity ranges are obtained by varying LPN deployments.

In the DL, the test case realistic network evaluation supports the numerical result. The best user throughput for DUDe is obtained when $\alpha = 2.5$ at which the decoupled association has the highest probability. Generally, the coupled-MC, coupled-LPN and DUDe associations gives performances that goes with Theorem 1 in the DL as performance corresponds to the most likely association cases. However, the UL throughput performance differs from the numerical evaluation in that the coupled-LPN association offers higher performance for $\alpha > 1$ compared to both DUDe and coupled-MC. We attribute the reason for the UL performance deviation from Theorem 1 to the propagation environment (differences in PLE from the assumption) and test case deployment scenario, which may not accurately represent Poisson random network.

Cell-edge user data rates

Similar setting with the above is considered for both DL and UL cell-edge performance evaluations (see Figs. 11 and 12). Again, the DL throughput performance from the realistic network evaluation is in agreement with Theorem 1, as the highest performances correspond to the most likely association cases. However, the UL performance deviates as it gives higher throughput in the case of coupled-LPN compared to other association cases.

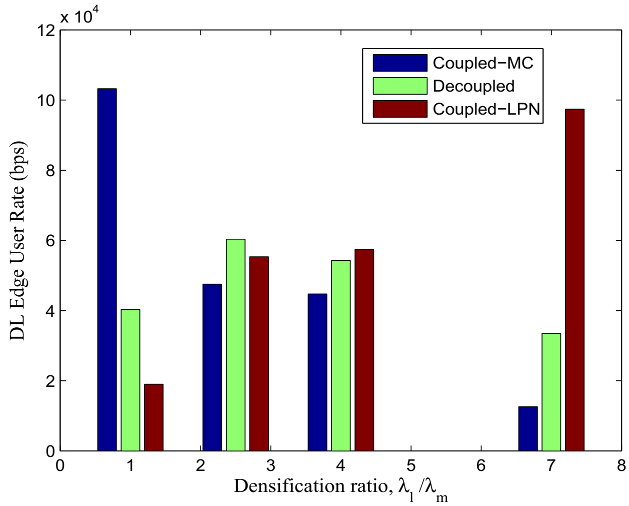

Fig. 11 DL cell-edge user rate at different densification ratios, $\lambda_m = 4/Km^2$

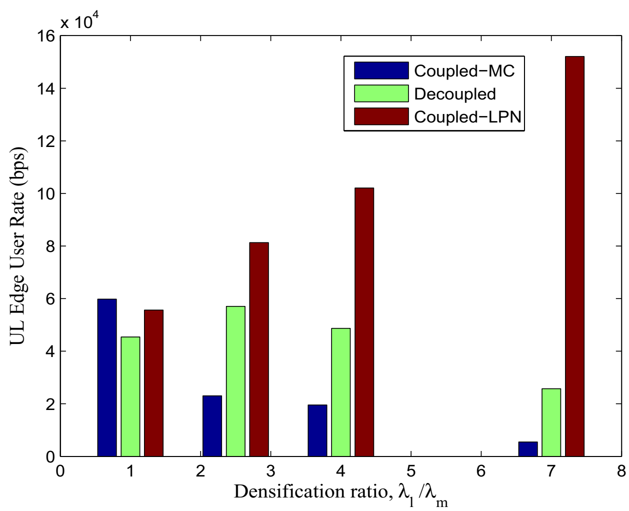

Fig. 12 UL cell-edge user rate at different densification ratios, $\lambda_m = 4/Km^2$

8 Conclusions

Aggressive offloading of UEs from MC to LPN is the well established approach for load balancing in HetNets with coupled sub-optimal user association. However, as node intensity increases the serving node becomes much closer to the UE. Therefore, the relative intensity at each tier can be used to parallel the effect of transmit power differences and to reduce the required load balancing effort. In ultra-dense heterogeneous wireless networks, the load distribution among different tiers changes with relative intensity ratios where different load balancing and interference coordination is required. Also, the user association choices impact the network performance differently for different relative intensities of nodes at each tiers.

In this paper, we presented different critical densification levels at which fair load distributions are obtained at different tiers. The main result is that different relative node intensity can be considered for the choices of flexible user association schemes. For smaller relative intensity (or $\alpha < \frac{\bar{P}^{\frac{2}{\gamma_l}}}{\bar{P}^{\frac{2}{\gamma_l}}-2}$), coupled association to the tier-1 is preferred by users. In this sub-optimal association and offloading with appropriate interference coordination can be used to enhance capacity. For a medium relative intensity level ($\frac{\bar{P}^{\frac{2}{\gamma_l}}}{\bar{P}^{\frac{2}{\gamma_l}}-2} \leq \alpha \leq \bar{P}^{\frac{2}{\gamma_l}} - 2$), users prefer the decoupled association. At higher relative intensity ($\alpha > \bar{P}^{\frac{2}{\gamma_l}} - 2$), users choose to associate to the tier-2 both in UL and DL. Realistic network evaluation needs additional research taking into account various deployment scenarios. The result has shown that there are cases for large PLE, like in dense urban deployment, where the decoupled association window becomes narrow and coupled association to LPNs gives the best user throughput. In this case, other capacity enhancement and mobility support approaches are required which will be part of the future work.

Appendix

Proof of Lemma 3—UL Ergodic Rates

When a typical UE is associated to the MC in the UL, the ergodic rate is given by:

$$\begin{aligned} R_{UL}^m &= \frac{1}{\ln(2)} \mathbf{E}_{r,\psi}[\ln(1 + \psi_{UL}^m)] \\ &= \frac{1}{\ln(2)} \int_0^\infty \mathbf{E}_\psi[\ln(1 + \frac{P_u h_m r^{-\gamma_m}}{I})] \cdot f(r,1) dr, \end{aligned} \quad (21)$$

where $I = \sum_{k \in \Phi_u \backslash u} P_u g_k x^{-\gamma_k}$ is the interference from users except the typical user at the origin and $f(r, 1)dr$ is the distance distribution of the serving node given in (1). The expectation of the spectral efficiency term in right-hand side (RHS) of (21) can be obtained as in [23].

$$
\begin{aligned}
R_{UL}^{m*} =&\mathbf{E}_{\psi}[\ln(1+\frac{P_u h_m r^{-\gamma_m}}{I})] \\
=&\int_0^\infty \mathbf{P}\{\ln(1+\frac{P_u h_m r^{-\gamma_m}}{I})>y\}dy \\
=&\int_0^\infty \mathbf{P}\{h_m > IP_u^{-1}r^{\gamma_m}(e^y-1)\}dy \\
\overset{a}{=}&\int_0^\infty \exp\{-\mu IP_u^{-1}r^{\gamma_m}(e^y-1)\}dy \\
=&\int_0^\infty \mathcal{L}_I\{\mu P_u^{-1}r^{\gamma_m}(e^y-1)\}dy
\end{aligned} \tag{22}
$$

Where (a) follows from the exponentially distributed h_m with mean $1/\mu$ and the Laplace Transform (LT) of the interference can be expressed as:

$$
\begin{aligned}
\mathcal{L}_I(s) &= \mathbf{E}_{\Phi_u,g_k}[e^{-sI}] \\
&= \mathbf{E}_{\Phi_u,g_k}[\exp\{-s\sum_{k\in\Phi_u\backslash u} P_u g_k x^{-\gamma_k}\}] \\
&= \mathbf{E}_{\Phi_u,g_k}[\prod_{k\in\Phi_u\backslash u}\exp\{-sP_u g_k x^{-\gamma_k}\}] \\
&\overset{a}{=}\mathbf{E}_{\Phi_u}[\prod_{k\in\Phi_u\backslash u}\mathbf{E}_{g_k}[\exp\{-sP_u h_k x^{-\gamma_k}\}]]
\end{aligned} \tag{23}
$$

(a) follows from the independence between Φ_u and g_k. With help of Probability Generating Functional (PGFL) [24] and [25] of the PPP, which states for some function $f(x)$ that $\mathbf{E}[\prod_{x\in\Phi}f(x)]=\exp\{-\lambda\int_{R^2}(1-f(x))dx\}$, the equation in (23) becomes:

$$
\begin{aligned}
\mathcal{L}_I(s) &= \mathbf{E}_{\Phi_u,g_k}[e^{-sI}] \\
&= \exp\{-2\pi\lambda_u\int_r^\infty(1-\mathbf{E}_{g_k}\left[\exp\{-sP_u g_k x^{-\gamma_k}\}\right])xdx\} \\
&\overset{a}{=}\exp\{-2\pi\lambda_u^*\int_r^\infty\left(1-\frac{\mu}{sP_u x^{-\gamma_k}+\mu}\right)xdx\}
\end{aligned} \tag{24}
$$

Where (a) follows from exponential distribution of g_k. Substituting $s=\mu P_u^{-1}r^{\gamma_m}(e^y-1)$ and putting (24) in (22) and (21) with simplification gives the result.

The same procedure can be followed to obtain the ergodic user rate when a typical UE is associated to the LPN in the UL, the ergodic rate is given by (19).

Proof of Lemma 4—DL Ergodic Rates

When a typical UE is associated to the MC in the DL, the ergodic rate is given by:

$$
\begin{aligned}
R_{DL}^{m} =&\frac{1}{\ln(2)}\mathbf{E}_{r,\psi}[\ln(1+\psi_{DL}^m)] \\
=&\frac{1}{\ln(2)}\int_0^\infty \mathbf{E}_{\psi}[\ln(1+\frac{P_m h_m r^{-\gamma_m}}{I})]\cdot f(r,1)dr,
\end{aligned} \tag{25}
$$

where $I=\sum_{k\in\Phi_m\backslash m}P_m g_k r^{-\gamma_k}+\sum_{k\in\Phi_l}P_l g_k r^{-\gamma_k}$ is the interference from MCs and LPNs to a typical user at the origin which being served by MC m and $f(r,1)dr$ is the distance distribution of the serving node. The expectation of the spectral efficiency term in RHS of (25) can be obtained as follows.

$$
\begin{aligned}
R_{DL}^{m*} =&\mathbf{E}_{\psi}\left[\ln\left(1+\frac{P_m h_m r^{-\gamma_m}}{I}\right)\right] \\
=&\int_0^\infty \mathbf{P}\{\ln\left(1+\frac{P_m h_m r^{-\gamma_m}}{I}\right)>y\}dy \\
=&\int_0^\infty \mathbf{P}\{h_m > IP_m^{-1}r^{\gamma_m}(e^y-1)\}dy \\
\overset{a}{=}&\int_0^\infty \exp\{-\mu IP_m^{-1}r^{\gamma_m}(e^y-1)\}dy \\
=&\int_0^\infty \mathcal{L}_I\{\mu P_m^{-1}r^{\gamma_m}(e^y-1)\}dy,
\end{aligned} \tag{26}
$$

where (a) follows from the exponentially distributed h_m with mean $1/\mu$. The LT of the interference can be expressed as:

$$
\begin{aligned}
\mathcal{L}_I(s) =&\mathbf{E}_{\Phi_m,\Phi_l,g_k}[e^{-sI}] \\
=&\mathbf{E}_{\Phi_m,\Phi_l,g_k}[\exp\{-s(\sum_{k\in\Phi_m\backslash m}P_m g_k r^{-\gamma_k} \\
&+\sum_{k\in\Phi_l}P_l g_k r^{-\gamma_k})\}] \\
=&\mathbf{E}_{\Phi_m,\Phi_l,g_k}[\prod_{k\in\Phi_m\backslash m}\exp\{-sP_m g_k r^{-\gamma_k}\} \\
&\times\prod_{k\in\Phi_l}\exp\{-sP_l g_k r^{-\gamma_k}\}] \\
\overset{a}{=}&\mathbf{E}_{\Phi_m}[\prod_{k\in\Phi_m\backslash m}\mathbf{E}_{g_k}[\exp\{-sP_m g_k r^{-\gamma_k}\}]] \\
&\times\mathbf{E}_{\Phi_l}[\prod_{k\in\Phi_l}\mathbf{E}_{g_k}[\exp\{-sP_l g_k r^{-\gamma_k}\}]]
\end{aligned} \tag{27}
$$

(a) follows from the independence between Φ_u,Φ_l and h_k. With help of PGFL [24] and [25] of the PPP, which states for some function $f(x)$ that $\mathbf{E}[\prod_{x\in\Phi}f(x)]=\exp\{-\lambda\int_{R^2}(1-f(x))dx\}$, and considering exponential distribution of g_k equation in (27) becomes:

$$
\begin{aligned}
\mathcal{L}_I(s) =&\mathbf{E}_{\Phi_m,\Phi_l,h_k}[e^{-sI}] \\
&= \exp\left\{-2\pi\lambda_m\int_r^\infty\left(1-\frac{\mu}{sP_m x^{-\gamma_k}+\mu}\right)xdx\right\} \\
&\times\exp\left\{-2\pi\lambda_l\int_r^\infty\left(1-\frac{\mu}{sP_l z^{-\gamma_k}+\mu}\right)zdz\right\}
\end{aligned} \tag{28}
$$

Substituting $s=\mu P_m^{-1}r^{\gamma_m}(e^y-1)$ and putting (28) in (26) and (25) with simplification gives the result.

Similarly, the same procedure can be followed to obtain the ergodic user rate when a typical UE is associated to the LPN in the DL, the ergodic rate is given by (20).

Funding There was no funding the authors are provided with during the research work.

Declarations

Conflict of interest Authors declare no conflict of interest.

References

1. Y. Shi, E. Alsusa, and M. W. Baidas, A survey on downlink–uplink decoupled access: advances, challenges,and open problems. *Computer Networks*, Vol. **213**, 2022.
2. F. Boccardi, et al. Why to decouple the uplink and downlink in cellular networks and how to do it. IEEE Comm. Mag. (2016).
3. Hou, K., Xu, Q., Zhang, X., Huang, Y. & Yang, L. User Association and Power Allocation Based on Unsupervised Graph Model in Ultra-Dense Network (2021).
4. Ge, X., Tu, S., Mao, G., Wang, C.-X. & han, T. 5G Ultra-Dense Cellular Networks. IEEE Wireless Comm. **23** (1), 72–79 (2016) .
5. Smiljkovikj, K., Popovski, P. & Gavrilovska, L. Analysis of the Decoupled Access for Downlink and Uplink in Wireless Heterogeneous Networks. IEEE Wireless Comm. Letters 4 (2), 173–176 (2015).
6. Sial, M. N. & Ahmed, J. A Realistic Uplink-Downlink Coupled and Decoupled User Association Technique forK-tier 5G HetNets. Arabian Journal for Science and Engineering (2018) .
7. Haddad, M., Więcek, P., Sidi, H. & Altman, E. An Automated Dynamic Offset for Network Selection in Heterogeneous Networks. IEEE Trans. on Mobile Comp. 15 (9), 2151–2164 (2015).
8. Muhammad, F., Abbas, Z. H., Abbas, G. & Jiao, L. Decoupled Downlink-Uplink Coverage Analysis with Interference Management for Enriched Heterogeneous Cellular Networks. IEEE Access 4, 6250–6260 (2016).
9. Saimler, M. & Coleri, S. Multi-Connectivity based Uplink/Downlink decoupled Energy Efficient User Association in 5G Heterogenous CRAN. IEEE Comm. Letters (2020).
10. Huang, T., Zheng, F.-C. & Lai, L. On the local delay and energy efficiency under decoupled uplink and downlink in HetNets. Sci. China Inf. Sci. 65 (132304), 1–10 (2022). doi: 10.1007/s11432-021-3306-4.
11. Wang, H., Garcia-Lozano, M., Mutafungwa, E., Yin, X. & Ruiz, S. Performance Study of Uplink and Downlink Splitting in Ultradense Highly Loaded Networks. Wireless Communications and Mobile Computing, Hindawi **2018** (2018) .
12. Sattar, Z., Evangelista, J. V., Kaddoum, G. & Batani, N. Spectral Efficiency Analysis of the Decoupled Access for Downlink and Uplink in Two Tier Network. IEEETrans. on Vehicular Technology 1–13 (2019). arXiv:1808.02523v2.
13. Shi, Y. 5G and Beyond Wireless Networkd Optimization Through Uplink and Downlink Decoupled Access. Ph.D. thesis, School of Electrical and Electronic Engineering, University of Manchester (2021).
14. Feng, Z., Feng, Z., Li, W. & Chen, W. Downlink and Uplink Splitting User Association inTwo-tier Heterogeneous Cellular Networks, 4659–4664 (2014).
15. Feng, Z., Feng, Z. & Gulliver, T. A. Joint user association and resource partition for downlink-uplink decoupling in multi-tier HetNets. Frontiers of Information Technology & Electronic Engineering 18 (6), 817–829 (2017).
16. Jiao, L. et al. Spectral Efficiency Analysis of Uplink-Downlink Decoupled Access in C-V2X Networks, 2062–2067 (2022).
17. Pardo, E. Study of Decoupled Uplink and Downlink Access In 5G Heterogeus systems. Master's thesis, King's College London and Universitat politécnica de Catalunya (UPC) (2016).
18. Sial, M. N. & Ahmed, J. Analysis of K-tier 5G heterogeneous cellular network with dual-connectivity and uplink-downlink decoupled access. Telecommun Syst (2017) .
19. Lahad, B., Ibrahim, M., Lahoud, S., Khawam, K. & Martin, S. Joint Modeling of TDD and Decoupled Uplink/Downlink Access in 5G HetNets With Multiple Small Cells Deployment. IEEE Trans. on Mobile Computing 20 (7), 2395–2411 (2021). DOI: 10.1109/TMC.2020.2979447.
20. Bhatti, O. W. et al. Performance Analysis of Decoupled Cell Association in Multi-Tier Hybrid Networks using Real Blockage Environments. arXiv:1705.04390v1 [cs.IT] (2017) .
21. Moltchanov, D. Distance distributions in random networks. Ad Hoc Networks 10 (6), 1146–1166 (2012). DOI: 10.1016/j.adhoc.2012.02.005.
22. Rappaport, T. S., George R. MacCartney, J., Samimi, M. K. & Sun, S. Wideband Millimeter-Wave Propagation Measurements and Channel Models for Future Wireless Communication System Design. IEEE Trans. on Comm. 63 (9), 3029–3056 (2015).
23. Andrews, J. G., Baccelli, F. & Ganti, R. K. A Tractable Approach to Coverage and Rate in Cellular Networks. IEEE Trans. on Comm. 59 (11), 3122–3134 (2011).
24. Kingman, J. Poisson Processes Oxford Studies in Probability (Oxford University, 1993).
25. Daley, D. & Vere-Jones, D. An Introduction to the Theory of Point Processes: Volume I: Elementary Theory and Methods Second edition edn, Vol. 1 of A Series of the Applied Probability Trust (Springer, 2003).

Dinkisa Bulti received his MScDegree in Computer Engineering and BSc Degree in Electrical andComputer Engineering from Addis Ababa University in 2011 and 2009,respectively. He has been working as a lecturer in the Department ofElectrical and Computer Engineering, Wolkite University, Ethiopiasince 2011. He also served as Dean of the College of Computing andInformatics, Wolkite University. Currently, he is pursuing his PhDdegree in Wireless Communications. His research interest includesMultimedia processing and communications, 5G mobile communications,Radio Resource Management, Network Planning and optimization, andWireless Sensor Networks.

Yihenew Wondie received his PhDDegree in Electrical Engineering and Computer Science, specializingin Communication Engineering from Kumamoto University of Japan in 2015. Since 2015, he has been serving in Addis Ababa Institute ofTechnology (AAiT). He authored more than 35 papers in reputablejournals and proceedings. His research interests include almost alladvances in wireless communications such as massive MIMO, mmWaveComminications, Cooperative wireless communications, Distributedantenna systems, Precoding and multiplexing techniques in 5G andbeyond. He is a member of IEEE.